

## Supporting Information for

### “Experimental determination of the curvature-induced intra-wall polarization of inorganic nanotubes”

Marie-Claire Pignié,<sup>a</sup> Sabyasachi Patra,<sup>a</sup> Lucie Huart,<sup>a</sup> Aleksandar R. Milosavljević,<sup>b</sup> Jean Philippe Renault,<sup>a</sup> Jocelyne Leroy,<sup>a</sup> Christophe Nicolas,<sup>b</sup> Olivier Sublemontier,<sup>a</sup> Sophie Le Caër<sup>a\*</sup> and Antoine Thill<sup>a\*</sup>

<sup>a</sup>NIMBE, UMR 3685 CEA, CNRS, Université Paris-Saclay, CEA Saclay 91191 Gif-sur-Yvette Cedex, France

<sup>b</sup>Synchrotron SOLEIL, L’Orme des Merisiers, Saint-Aubin, BP 48, 91192 Gif-sur-Yvette Cedex, France.

\*corresponding authors: [sophie.le-caer@cea.fr](mailto:sophie.le-caer@cea.fr) and [antoine.thill@cea.fr](mailto:antoine.thill@cea.fr)

### Characterization of imogolites samples by Cryo-TEM

A 5  $\mu\text{L}$  drop of the aqueous imogolite suspension ( $\sim 80 \text{ mg.L}^{-1}$ ) was deposited on an electron microscopy grid covered with a holey carbon film (Quantifoil R2/2) previously treated with a plasma glow discharge. The excess liquid on the grid was soaked up with a filter paper, and the grid was then quickly immersed in liquid ethane to form a thin vitreous ice film. The overall procedure was executed using a Vitrobot apparatus (FEI Company). The microscopic observations were made at low temperature ( $-180^\circ\text{C}$ ) on a JEOL 2010 FEG microscope operated at 200 kV. A Gatan camera was used to collect the images.

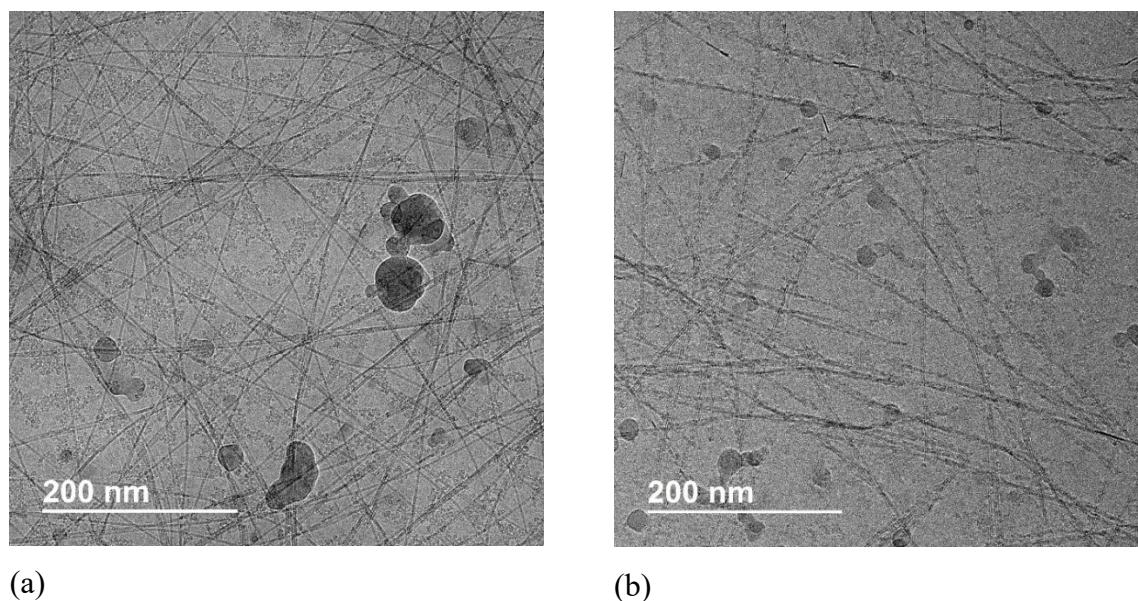


**Figure SI-1.** Cryo-TEM images of (a) IMO-OH and of IMO-CH<sub>3</sub> nanotubes.

## Characterization of imogolite samples by Fourier-Transform InfraRed spectroscopy (FT-IR)

FT-IR spectra were obtained from imogolite (1% by mass) dispersed in KBr pellets. The powder was compacted into thin self-supporting discs for IR transmission studies by applying a pressure of about  $10^9$  Pa for five minutes. All the spectra were obtained from 100 scans accumulated with a Bruker Tensor 27 FT-IR spectrophotometer operating with  $4\text{ cm}^{-1}$  resolution (Figure SI-2). The wavenumber range was  $370\text{-}4000\text{ cm}^{-1}$ . The background was subtracted in all cases. The assignment of the bands (Table SI-1) confirm that the samples are IMO-OH and IMO-CH<sub>3</sub>, respectively.

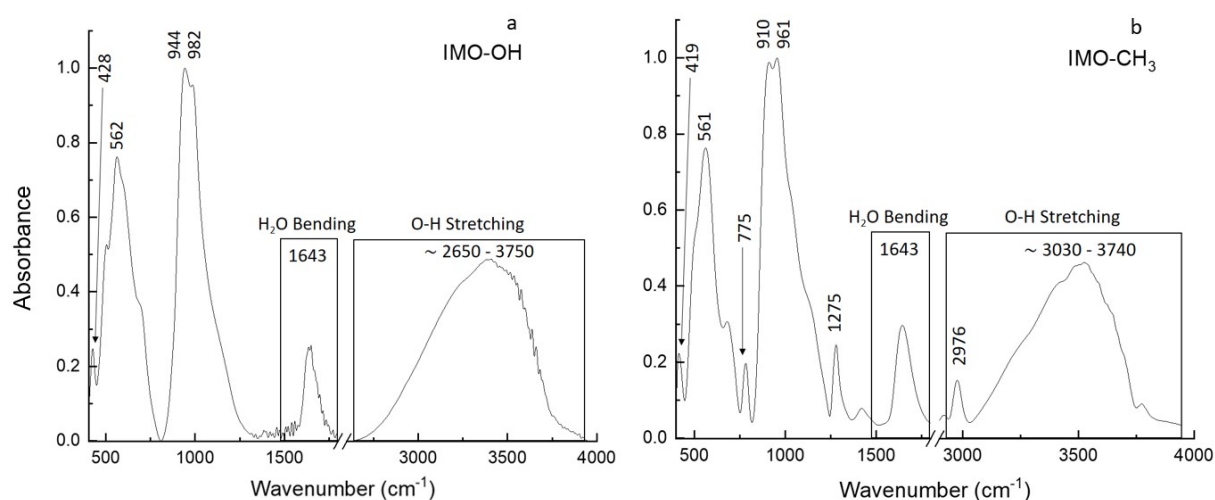


**Figure SI-2.** (a) FT-IR spectra of IMO-OH (a) and (b) IMO-CH<sub>3</sub>

Band assignment	Wavenumber (cm <sup>-1</sup> )	
	IMO-OH	IMO-CH <sub>3</sub>
CH <sub>3</sub> asymmetric stretching	-	2976
Si-CH <sub>3</sub> methyl symmetric deformation	-	1275
Methyl rocking and Si-C stretching	-	775
Si-O stretching	944 & 982	910 & 961
Al-O modes	562	561
H <sub>2</sub> O bending	1640	1643
O-H stretching	2700-4000	3000-4000

**Table SI-1.** Band assignment for the infrared bands observed in IMO-OH & IMO-CH<sub>3</sub>.<sup>1</sup>

## Size distribution of NTs agglomerates in the aerosols

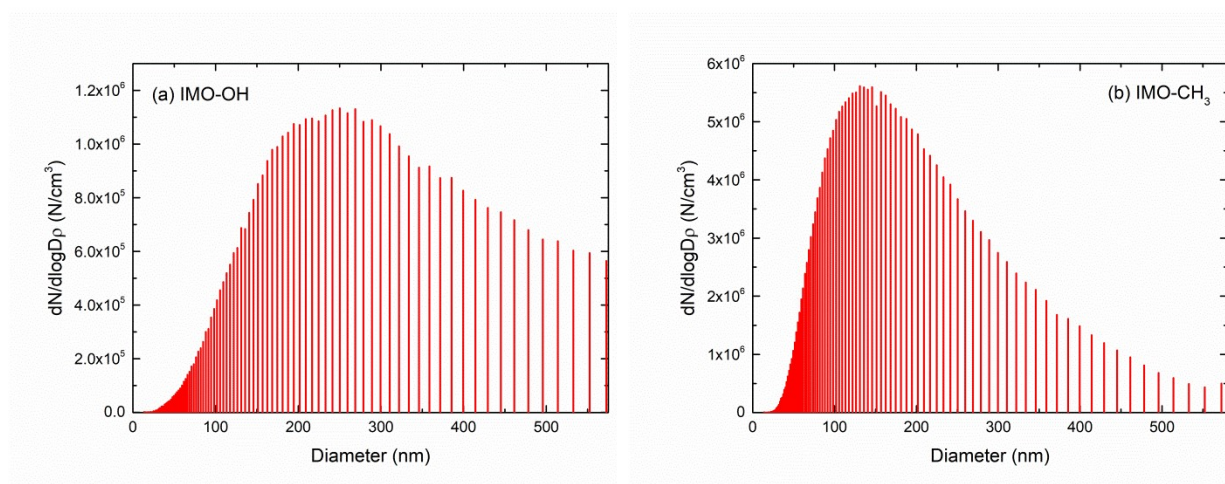


**Figure SI-3.** Size distribution of the nanotubes agglomerates in the aerosol for (a) IMO-OH and (b) IMO-CH<sub>3</sub>.

## Complementary results and discussion

### C 1s core level spectra obtained from synchrotron radiation-based XPS experiments on isolated nanotubes agglomerates

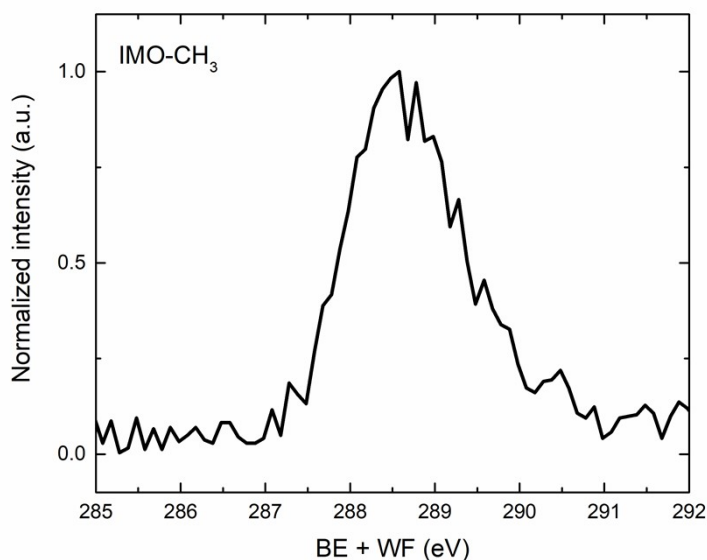


**Figure SI-4.** Normalized synchrotron radiation based XPS C 1s core-level spectrum for IMO-CH<sub>3</sub>. The incident energy of the photons was 400 eV. No C 1s spectra could be measured in the case of IMO-OH, evidencing that no adventitious carbon was present in this sample. The maximum of the C 1s core level spectrum is located at 288.6 eV. By subtracting the WF of IMO-CH<sub>3</sub>, which is equal to 4.45 eV, we get a binding energy of 284.15 eV, a reasonable value for a methyl group linked to a silicon atom. For instance, in SiC, the C 1s binding energy was reported at 283.3 eV.<sup>2</sup>

### Calculation of the thickness of the water layer on IMO-CH<sub>3</sub> NTs containing eosin Y (isolated samples)

The Al 2p core-level spectra were measured for two incident photon energies (150 and 400 eV). The area of the Al 2p contribution was then normalized with respect to the photon flux, the number of sweeps during the measurements, and the respective photoionization cross sections for Al 2p at 150 and 400 eV, respectively. PENELOPE simulation code<sup>3</sup> allows

obtaining:  $\frac{\sigma_{Al2p, 150eV}}{\sigma_{Al2p, 400eV}} = 9.9$ . The ratio of the Al 2p contribution for the incident photon energies of 150 eV and 400 eV is thus calculated to be equal to 0.03.

Assuming that:

$$\frac{A_{Al2p, 150eV, norm}}{A_{Al2p, 400eV, norm}} = 0.03 = \exp\left(-d\left(\frac{1}{L_{150}} - \frac{1}{L_{400}}\right)\right)$$

with  $d$  the water thickness of the surface of the particles, and  $L_{150}$  and  $L_{400}$  the electron attenuation length in ice for incident photons of 150 eV and 400 eV, corresponding to a kinetic energy of Al 2p photoelectrons roughly equal to 70 eV and 320 eV, respectively. We get  $L_{150} \sim 1$  nm and  $L_{400} \sim 1.5$  nm in reference.<sup>4</sup> The water thickness  $d$  is then calculated to be roughly equal to 10 nm.

### **O 1s core level spectra obtained from synchrotron radiation-based XPS experiments on isolated nanotubes agglomerates**

The O 1s normalized core level spectra measured for both imogolites on isolated nanotubes are shown in Figure SI-5. These results were obtained with 600 eV energy photons. The same results were obtained with 900 eV energy photons. The peak at 540.6 eV corresponds to water vapor. Obviously, the two spectra are very similar for both imogolites. However, supplementary oxygen contributions are present in IMO-OH as compared to IMO-CH<sub>3</sub>, i.e. -OH groups covering the internal surface of the tubes together with internal water molecules. All these contributions should be probed under our experimental conditions. Obviously, not being able to detect any difference between the two spectra suggests that the oxygen signal is dominated by the external water present on the surface of the nanoparticles.

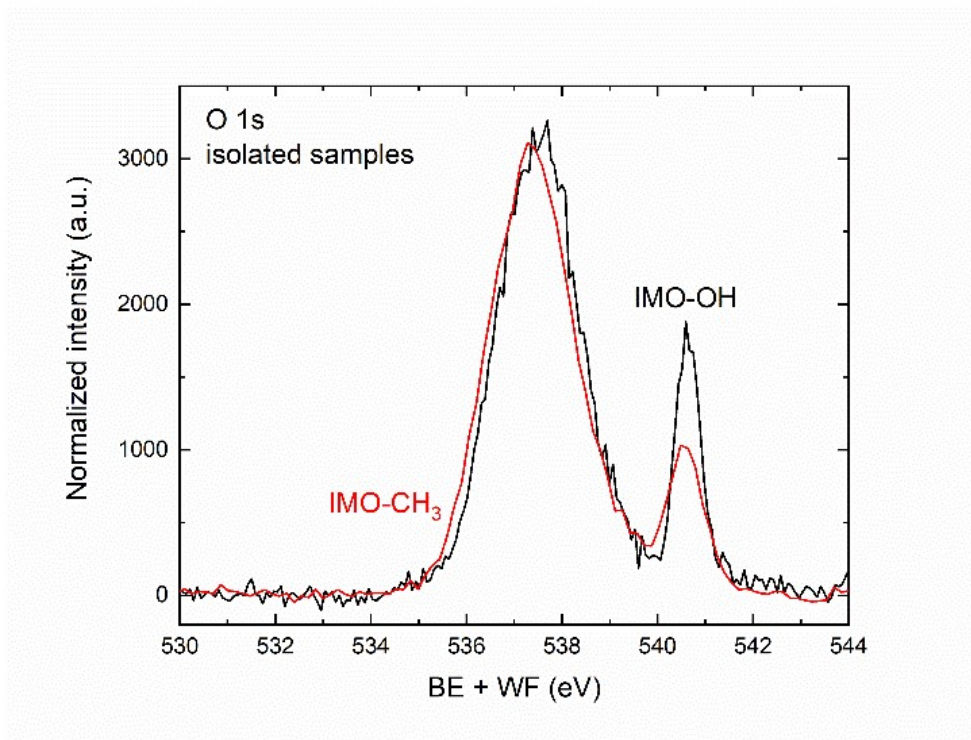


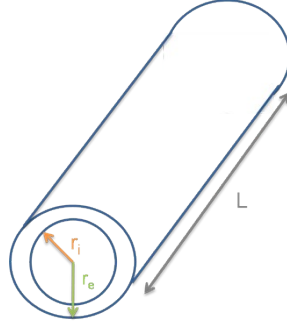
**Figure SI-5.** Normalized synchrotron radiation based XPS O 1s core-level spectra for IMO-OH (black) and IMO-CH<sub>3</sub> (red). The incident energy of the photons was 600 eV. The total resolution is 550 meV for IMO-OH and 870 meV for IMO-CH<sub>3</sub>. The peak at 540.6 eV corresponds to water vapor. Same results were obtained for 900 eV energy photons (data not shown).

### Electric field in the imogolite wall

In this discussion, imogolite is considered as a cylindrical capacitor. The internal and external surface of the nanotubes are negatively and positively charged, respectively. The corresponding charges are labelled as  $Q_i$  and  $Q_e$ , respectively, with  $\sigma_i$  and  $\sigma_e$  the internal and external surface density of charge (see Scheme SI-1):

$$Q_i = \sigma_i 2\pi r_i L \text{ with } \sigma_i < 0$$

$$Q_e = \sigma_e 2\pi r_e L \text{ with } \sigma_e > 0 \text{ (Eq. 1)}$$



**Scheme SI-1.** Scheme of a nanotube, with its internal and external radius ( $r_i$  and  $r_e$ , respectively). Length  $L$  is much greater than  $r_i$  and  $r_e$ .

As there is no net charge in the system,  $\sigma_i$  can be expressed as a function of  $\sigma_e$ :

$$\sigma_i = -\frac{r_e}{r_i}\sigma_e \quad (\text{Eq. 2})$$

Gauss' law states that the flux of the electric field out of a closed surface is proportional to the electric charge enclosed by the surface. In our case, the electric field is thus equal to zero inside the cavity of the nanotube and outside the nanotube, as there is no net charge. Within the imogolite wall, due to symmetry, the electric field has only a radial component:  $\vec{E}$  is directed radially everywhere.

$$r < r_i \text{ or } r \geq r_e \quad E = 0$$

$$\text{for } r_i \leq r < r_e, \quad \oiint \vec{D} d\vec{S} = Q \quad (\text{Eq. 3})$$

$$\text{with } \vec{D} \text{ the electric displacement field: } \vec{D} = \epsilon_0 \epsilon_r \vec{E} \quad (\text{Eq. 4})$$

$\epsilon_r$  is the relative permittivity of imogolite and  $\epsilon_0$  is the permittivity of vacuum.

$$\text{From Eqs. 3-4, we get: } \frac{Q}{\epsilon_0 \epsilon_r} = \frac{\sigma_i 2\pi r_i L}{\epsilon_0 \epsilon_r} = E(r) 2\pi r L \quad (\text{Eq. 5})$$

Indeed, the electric field is perpendicular to the side of the Gauss surface (which is a cylinder) and its intensity is uniform on this surface.

$$\text{Therefore, } E(r) = \frac{\sigma_i r_i}{\epsilon_0 \epsilon_r r} \quad (\text{Eq. 6})$$

$$V(r) = \frac{-\sigma_i r_i}{\epsilon_0 \epsilon_r} \ln(r) + A$$

The potential  $V(r)$  is thus equal to: (Eq. 7),  $A$  being an integration constant. The sum of the kinetic energy ( $E_{kin}$ ) and of the electric potential energy ( $qV(r)$ , with  $q$  the charge) being constant, we get:

$$E_{kin}(r_i) + qV(r_i) = E_{kin}(r_e) + qV(r_e) \quad (\text{Eq. 8})$$

$$\Delta E_{kin} = E_{kin}(r_e) - E_{kin}(r_i) = \frac{-q\sigma_i r_i}{\epsilon_0 \epsilon_r} \ln\left(\frac{r_i}{r_e}\right) \quad (\text{Eq. 9})$$

Therefore, the kinetic energy gained by a photoelectron ejected out of the nanotube is equal to

$$\frac{e\sigma_i r_i}{\epsilon_0 \epsilon_r} \ln\left(\frac{r_i}{r_e}\right) \quad (\text{Eq. 10}).$$

The relative permittivity  $\epsilon_r$  of imogolite can be assumed to range between 5 and 8 as in mica, which has a close chemical formula.<sup>5</sup>

In the case of IMO-OH,  $r_i = 9 \text{ \AA}$ ;  $r_e = 14.5 \text{ \AA}$ .

In the case of IMO-CH<sub>3</sub>,  $r_i = 10 \text{ \AA}$ ;  $r_e = 15.5 \text{ \AA}$ .

In the case of IMO-OH,  $\Delta E_{kin}$  is equal to 0.7 eV (as compared to kaolinite, see Figure 6 in the main text). From Eqs. 10 and 2, and by assuming that the relative permittivity  $\epsilon_r$  of IMO-OH is equal to 5, we get  $\sigma_e = 45 \text{ mC}\cdot\text{m}^{-2}$ , which is in excellent agreement with the value of 42  $\text{mC}\cdot\text{m}^{-2}$  given in reference.<sup>6</sup> The same calculations were also performed for IMO-CH<sub>3</sub>, with  $\Delta E_{kin}$  equal to 0.2 eV and assuming the same value for  $\epsilon_r$ , leads to a smaller  $\sigma_e$  value equal to 13  $\text{mC}\cdot\text{m}^{-2}$ .

## Valence spectra of imogolites and of water

Liquid experiments were also carried out at the PLEIADES beamline of SOLEIL Synchrotron, Saint-Aubin, France. The liquid jet set-up is described into details in reference 7. Liquid water valence spectra was recorded adding NaCl salts (0.05 M) in order to avoid electrokinetic charging of the liquid microjet.<sup>8</sup> The measurements were performed with photons of 100 eV of energy with a total experimental resolution of 70 meV. Data were energy-calibrated against the adiabatic ionization energy of the X 1b<sub>1</sub> state of H<sub>2</sub>O<sup>+</sup> at 12.6 eV in the gas phase.<sup>9-10</sup> The alignment of the state at 12.6 eV for both experiments (liquid jet and nanoparticles set-up, see the inset of Figure SI-6) evidences the calibration of the data. The photoionization threshold of water is extrapolated at  $10.10 \pm 0.07$  eV, which is in agreement with previous literature data.<sup>11-12</sup> The valence spectra obtained for water (with NaCl at 0.05 M concentration) and for both imogolites are given in Figure SI-6.

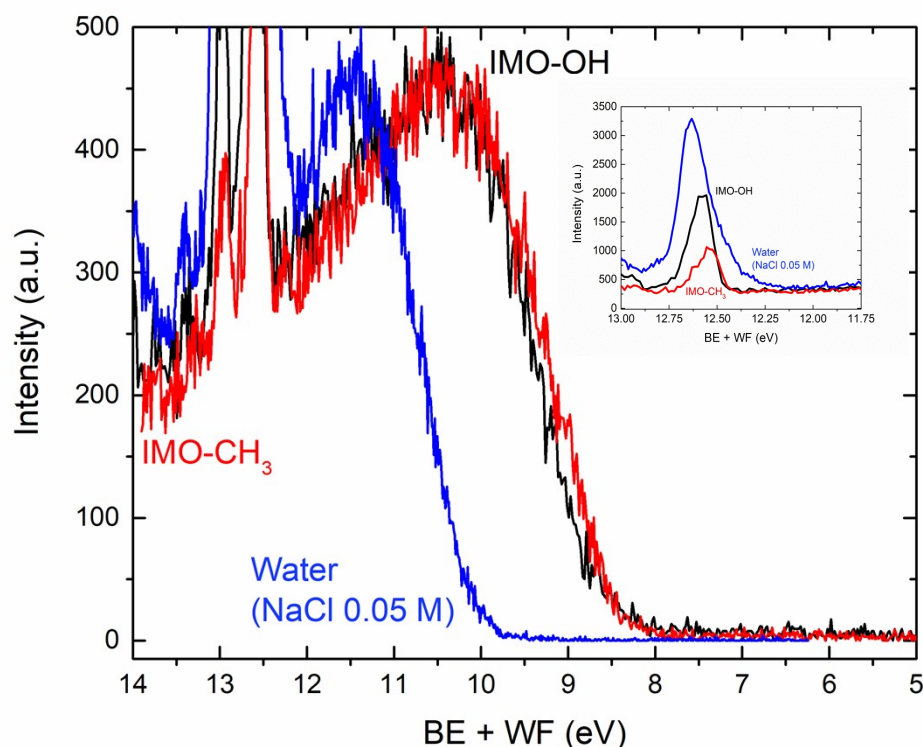


**Figure SI-6.** Valence spectra of IMO-OH (black), IMO-CH<sub>3</sub> (red) and water with 0.05 M of NaCl (blue) measured on the PLEIADES beamline of SOLEIL synchrotron using nanoparticles and liquid jets, respectively. The energy of the incident photons is equal to 100 eV. The inset shows the calibration of the data.

Valence spectra measured on deposited samples with a laboratory XPS set-up

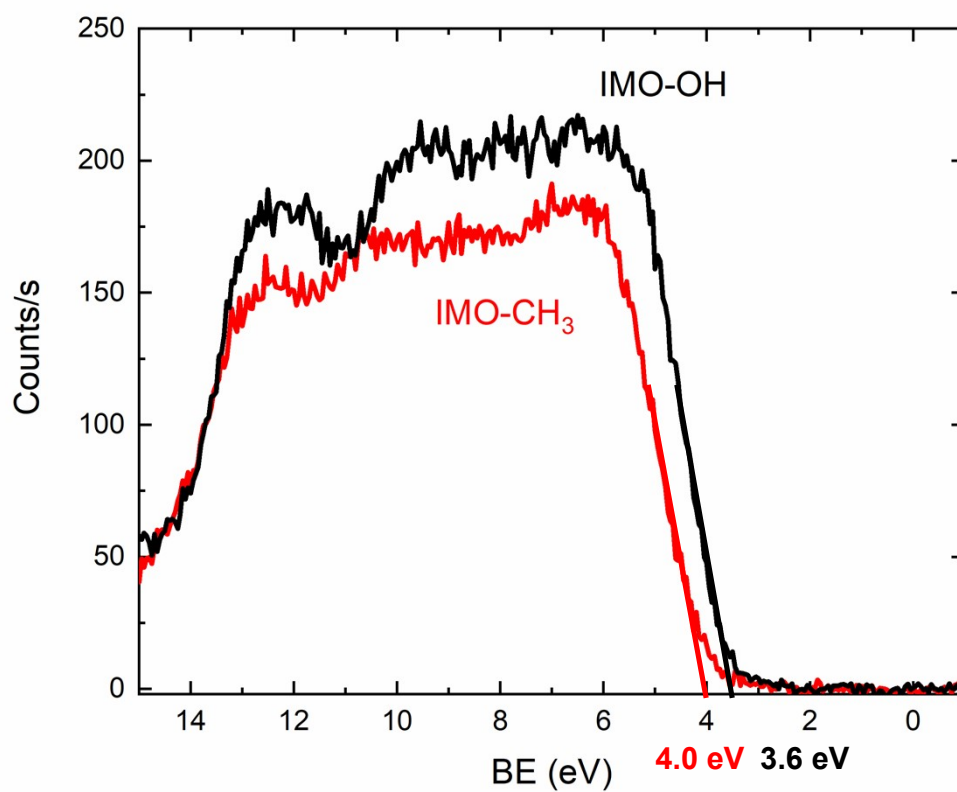


**Figure SI-7.** Valence spectra of IMO-OH (black) and IMO-CH<sub>3</sub> (red) measured on imogolite powder deposited on a carbon tape. The intercept of the linear fit with the x-axis is equal to 3.6 and 4.0 eV for IMO-OH and IMO-CH<sub>3</sub>, respectively.

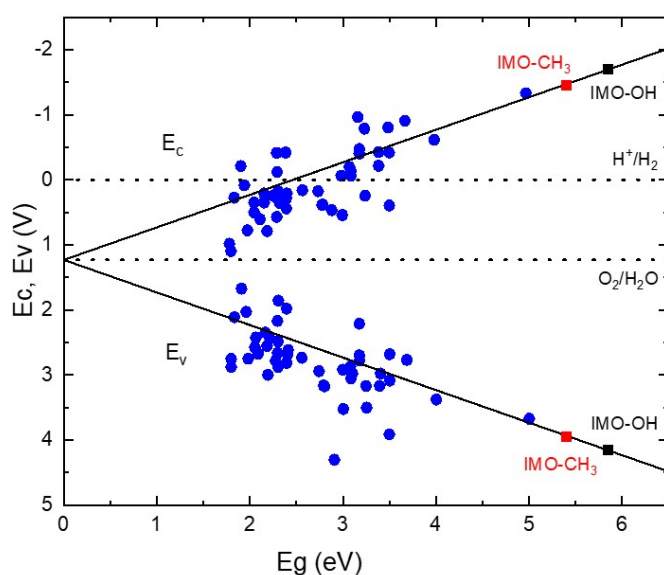
## Comparison of the band structure of imogolites and of other oxide semiconductors

Imogolite's band structure can be compared with a range of oxide semiconductors (Figure SI-8). The relationships between the valence ( $E_v$ ) and conduction ( $E_c$ ) band edges and the band gap ( $E_g$ ), expressed in eV, (Eqs. 11 and 12) determined for oxide semiconductors also apply to imogolites as demonstrated in Figure SI-8.<sup>13</sup>

$$E_c(V \text{ vs NHE}) = 1.23 - \frac{E_g}{2} \text{ (Eq. 11);}$$

$$E_v(V \text{ vs NHE}) = 1.23 + \frac{E_g}{2} \text{ (Eq. 12)}$$

Imogolites' band edges evidence the theoretical capability of these aluminosilicate NTs for water splitting (Figure SI-8) with a conduction band edge energy above the redox potential of  $H^+/H_2$  (0 V vs. NHE at pH 0) and a valence band edge energy below the redox potential of  $H_2O/O_2$  (+1.23 V vs. NHE at pH 0).



1

**Figure SI-8.** IMO-OH (black squares) and IMO-CH<sub>3</sub> (red squares) conduction ( $E_c$ ) and valence ( $E_v$ ) band edges compared with oxide semiconductors (blue circle). The evolution of conduction and valence band edges is consistent between oxide semiconductors and imogolites. The water potential domain is also depicted. See the article of Matsumoto<sup>13</sup> for more details.

## References

- 1 Y. Liao, P. Picot, M. Lainé, J.-B. Brubach, P. Roy, A. Thill and S. Le Caër, *Nano Res.*, 2018, **11**, 4759-4773.
- 2 M. Veres, M. Koos, S. Toth, M. Füle, I. Pocsik, A. Toth, M. Mohai and I. Bertoti, *Diamond & Rel. Mater.*, 2005, **14**, 1051-1056.
- 3 F. Salvat, J. M. Fernandez-Varea, E. Acosta and J. Sempau *Penelope- a Code System for Monte Carlo Simulation of Electron and Photon Transport*, Nuclear Energy Agency: 2001.
- 4 R. Signorell, *Phys. Rev. Lett.*, 2020, **124**, 205501.
- 5 Y. L. Ma and J. Karube, *Soil Sci. Plant Nutr.*, 2013, **59**, 125-129.
- 6 J. P. Gustafsson, *Clays Clay Miner.*, 2001, **49**, 73-80.
- 7 B. Winter, *Nucl. Instr. Methods Phys. Res. A*, 2009, **601**, 139-150.
- 8 N. Preissler, F. Buchner, T. Schultz and A. Lübcke, *J. Phys. Chem. B*, 2013, **117**, 2422-2428.
- 9 M. S. Banna, B. H. McQuaide, R. Malutzki and V. Schmidt, *J. Chem. Phys.*, 1986, **84**, 4739-4744.
- 10 X. Ren, S. Amami, K. Hossen, E. Ali, C. Ning, J. Colgan, D. Madison and A. Dorn, *Phys. Rev. A*, 2017, **95**, 022701.
- 11 B. Winter, R. Weber, W. Widdra, M. Dittmar, M. Faubel and I. V. Hertel, *J. Phys. Chem. A*, 2004, **108**, 2625-2632.
- 12 C. F. Perry, P. Zhang, F. B. Nunes, I. Jordan, A. von Conta and H. J. Wörner, *J. Phys. Chem. Lett.*, 2020, **11**, 1789-1794.
- 13 Y. Matsumoto, *J. Solid State Chem.*, 1996, **126**, 227-234.